Dynamic phases in a spring-block system

A. Johansen, P. Dimon, C. Ellegaard, J. S. Larsen, and H. H. Rugh
The Niels Bohr Institute, Blegdamsvej 17, DK-2100 Copenhagen, Denmark
(Received 2 August 1993)

When a block is pulled via a spring across a surface, there appear to be several different dynamic "phases." These can be characterized by the pulling velocity v_0 and a dynamic velocity $v_D = g\sqrt{m/k}$, where g is the acceleration of gravity, m is the mass of the block, and k is the spring constant. For sufficiently small v_0, the block displays stick-slip (relaxation) motion. Then, as a function of decreasing v_D, this stick-slip motion is first nearly periodic, then aperiodic with approximately an exponential slip size distribution, and then aperiodic with possibly a power-law slip size distribution. When v_0 is increased, the block eventually ceases to stick and just slides across the surface. The motion can then be adequately described by a Langevin model.

PACS number(s): 46.10.+z, 46.30.Pa, 62.20.−x, 05.40.+j

I. INTRODUCTION

The physics of nonlinear systems can often be surprising and unpredictable. In mechanical systems the nonlinear element may be friction, a force far more complicated than the one discussed in elementary physics texts. Suppose, for example, a block resting on a surface is attached to a spring, the other end of which is pulled at a constant velocity. At sufficiently slow velocities, it is observed that, "the sliding process is not a continuous one; the motion proceeds by jerks. The metallic surfaces 'stick' together until, as a result of the gradually increasing pull, there is a sudden break with a consequent very rapid 'slip' [1]." This intermittent behavior has been termed stick-slip (or relaxation) motion and is now established as a generic phenomenon of friction in overdamped systems [2–6]. This phenomenon is also reminiscent of fault seismicity [7] and for this reason attempts have been made to model earthquakes by spring-block systems with many degrees of freedom, both experimentally [8] and theoretically [8–14].

The results of an experiment with a single metal block on a dry metal surface will be presented [15]. Previously, systems with only a single degree of freedom have generally been studied with large loads in an engineering context [4,6]. (One exception is an experiment by Feeny and Moon who found chaos in a driven system [16].) As might be expected, it is found that the dynamics of a system with only one (apparent) degree of freedom is quite different from that displayed by systems with many degrees of freedom. Such systems generally show scale invariance and are possibly examples of self-organized criticality (SOC) [17, 18]. It has been suggested that the scale invariance found in earthquakes (see Appendix) is also an example of SOC [19, 20]. This has been supported experimentally in model systems by Burridge and Knopoff [8] who found scale invariance in a spring-block model by measuring the change in potential energy after each slip event, and by Feder and Feder [21] who measured the force required to drag sandpaper across a carpet. There may, however, be other possibilities. Computer simulations by Vasconcelos *et al.* [14] strongly suggest that the observed scaling represents only a portion of some more complicated dynamic phase diagram. We shall return to this idea at the end of the paper.

The paper is structured as follows. In Sec. II we review various relevant aspects of friction. The experiment is described in Sec. III and the methods of data analysis are given in Sec. IV. The results of the analysis are presented in Sec. V, followed by a discussion in Sec. VI.

II. SOME ASPECTS OF FRICTION

In this section we discuss the importance of contact area, surface geometry, and the normal degree of freedom in the context of our experiment. For a review of friction theory and stick-slip motion, see Refs. [2–6].

A. Static friction

Geometrically, one may view a material surface as being rough, consisting of asperities of different sizes which will deform under pressure [22]. If one surface is placed on top of another, the deformation will cease when the total yield pressure P_y of the asperities equals the load F_L of the upper surface divided by the total contact area A_c, i.e., $P_y = F_L/A_c$. This is the basic assumption of the well-known adhesion model for static friction of Bowden and Tabor [2], where the origin of the static friction is an (intermolecular) adhesion between the two surfaces at the points of contact.

Assuming plastic deformation, an estimate of the contact area A_c can be made by approximating $P_y \approx gH_B$ where g is the acceleration of gravity and H_B is the Brinell hardness. Thus for a metal block of height h and density ρ, and with $F_L = \rho ghA$ where A is the apparent area, we find that, typically,

$$A_c/A = \frac{\rho h}{H_B} \sim 10^{-6} , \tag{1}$$

where we have taken $h = 1$ cm, $\rho = 10$ g/cm^3, and $H_B = 10^7$ g/cm^2. Thus, even though the apparent area may be macroscopic, the contact area can be quite small. (Specifically, in our experiment $A \sim 1$ cm^2 so $A_c \sim 100$ μm^2.) Thus microscopic randomness may not

simply average out. This apparent stochastic element can result in strong fluctuations in the static friction so the classical friction law, where the friction force is proportional to the load, will only exist in an average sense.

B. Dynamic friction

Dynamic friction presents a different problem. Extensive experimental studies [2–6] have established that the velocity dependence is weak and nonlinear and has hysteresis. Attempts have been made to explain these features purely in the context of the adhesion model discussed in the previous section but only with limited success [4]. More recently, so-called state-variable friction laws have been introduced mainly on a phenomenological basis [24].

Both experiments and simulations, however, have demonstrated the importance of the normal degree of freedom [4], since as the velocity increases, there will be more momentum transfer into the normal direction, producing an upward force on the upper surface. This will result in an increase in the separation between the two surfaces, and hence a decrease in the contact area. From here one can either return to the adhesion model with a reduced contact area and hence reduced adhesion [4], or use the collisions between the asperities as the dissipation mechanism [25]. Both these models have been used with some success in explaining the observed behavior. They may also be used in connection with a Langevin model for the motion where the collisions are the source of the noise term. This will be discussed further in Sec. V D. An important consequence of this picture is that if the fluctuations in the static friction are indeed determined by surface geometry and contact area, then one should expect the dynamic friction to fluctuate for the same reasons. Again, this means that deterministic friction-velocity relations at best only exist in an average sense.

C. Stick-slip motion

When a block is pulled via a spring, one observes that as a function of the pulling velocity v_0, there are two distinct dynamics in the slow and fast limits [4]: stick-slip (relaxation) motion for sufficiently small v_0 and damped harmonic motion (i.e., continuous sliding) for sufficiently large v_0.

The stick-slip motion that has been observed previously is usually periodic or nearly so. This can be explained as follows. Since the loads are usually on the order of kilograms, the contact area [see Eq. (1)] will be on the order of square millimeters, which may result in less stochastic and more deterministic behavior. Given a narrow distribution of initial conditions, say, in the static friction, a deterministic equation of motion will always result in a (nearly) periodic motion. As a consequence, purely deterministic relations between stick-slip characteristics, such as amplitude and period, and experimental conditions have generally been used in modeling this phenomenon [4, 6]. In the present experiment, we used masses between $\sim$ 30 g and $\sim$ 700 g and in fact we observe a transition from aperiodic to nearly periodic motion when we switch to heavier loads. These results will be discussed further in Sec. V C.

For large v_0, the block no longer sticks to the surface and instead we observe continuous sliding. The dynamics become essentially that of a damped harmonic oscillator, although the motion is still not completely periodic. Again, this will be discussed further in Sec. V D.

Given what has been said above, it is difficult to find an equation of motion for stick-slip motion in the stochastic limit, let alone one that also describes the crossover to damped harmonic motion.

III. EXPERIMENTAL SETUP

The experimental setup is shown schematically in Fig. 1. The basic idea, as described in the Introduction, is very simple. In practice, however, it is far more convenient to keep one end of the spring fixed in the laboratory frame of reference and place the block on a rotating surface and hence obtain arbitrarily long time series. We therefore used a rotating table (1) driven by a rubber wheel (2). The wheel was connected to a gear box (3) with ratio settings from 1:1000 to 1:500 000 and which was driven by a 5000-rpm dc motor (4). The motor speed was kept constant throughout the experiment. Thus, by changing the gear ratio, we were able to obtain a range of effective pulling velocities v_0 from 0.016 mm/s to 8.0 mm/s.

Most of the work was conducted on the outer surface of a 32.5-cm-diam bearing made from SAE 52100 steel. On it was placed a 28.5-g block of dimensions $1 \times 1 \times 3$ cm^3 made from a work-hardened tool bit (5). Both surfaces were therefore smooth and robust. Larger masses were studied by placing weights on top of the block. We also studied brass and aluminum surfaces with a block of the same material. The aluminum surface was smoothed on a milling machine and the brass surface was simply cut. Although the steel surface was considerably smoother than the brass and aluminum surfaces, they all gave qualitatively the same results. One might expect that the much harder and smoother steel surface would diminish the importance of random processes, but this was not the case. The blocks and table surfaces were prepared by cleaning with isopropyl alcohol and then running the apparatus for about an hour before measuring.

The block was rigidly attached to a 4-cm plastic rod (6)

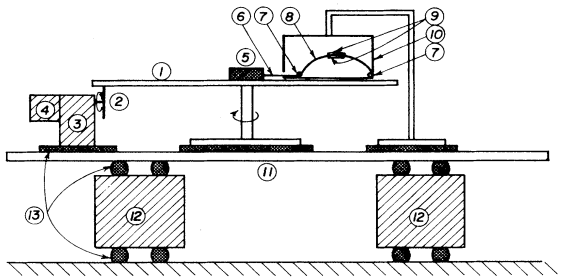

FIG. 1. A schematic sideview of the experimental setup (see text). The block rests near the perimeter of the table closest to the observer.

as close to the table surface as possible to prevent torquing. The rod was connected via a rotating joint (7) to a thin curved steel strip which served as a spring (8). The other end of the spring was fixed in the laboratory frame of reference to another rotating joint. The joints prevented the spring from lifting the block off the surface as its length changed. The equilibrium length of the spring was ~ 10 cm. The stiffness of the spring was chosen such that for the 28.5-g block, there was a reasonable signal from our transducers, but the spring would not be stretched beyond its linear limit. From direct calibration the spring constant was measured to be 22.4 N/m. We also studied the effect of using a stiffer spring (152 N/m) although this obviously restricted the range of motion of the block. The block and spring were aligned tangentially to the rotating surface near its perimeter. The size of the block was small enough compared to the diameter of the rotating surface that it moved nearly tangentially with no significant radial component.

Our transducer consisted of two nominally identical 350-Ω strain gauges which were glued to opposite sides of the spring at its midpoint (9). The gauges had a nominal response time of ~ 1 ms. The gauges comprised two arms of a Wheatstone bridge. To maximize our dynamic range, the bridge was balanced so that the shortest spring length during a measurement did not overload the lower output range of the preamplifier. The bridge was powered with a 12-V car battery. The spring, the gauges, and the bridge were all enclosed in an aluminum box (10) to shield against external noise. The battery was also enclosed in another aluminum box which formed part of the same common shield. Finally, in order to reduce mechanical vibrations, the table, the gearbox, and the transducer box were isolated from the floor by placing them on a heavy iron plate (11) resting on two bricks of concrete (12), with rubber pads (13) in between.

The signal from the bridge was connected to the differential inputs of a Stanford Research SR560 low-noise preamplifier. The bridge impedance (and hence the gauge resistance) was chosen to minimize the output noise from the preamplifier. The amplifier included a low-pass filter with a roll-off frequency of 100 Hz. The preamplifier output was connected to a Hewlett-Packard HP3562A dynamic signal analyzer (DSA) which was controlled from a personal computer.

The quality of the signal was checked by pinning the block to the surface and measuring the noise level with the dc motor both on and off. This tested for fluctuations in the motor speed, for noise generated by the motor, and for mechanical vibrations. No observable speed fluctuations or changes in the noise level could be found. This method also tested the linearity of the system which was better than 1% over a much wider range of spring displacements than actually used. The final signal-to-noise ratio was better than 1000:1 which corresponds to a detectable range of motion for the 28.5-g block with the 22.4-N/m spring of ~ 5 μm to ~ 5 mm.

IV. DATA ANALYSIS

As discussed in Sec. II C, there are two limiting cases for the dynamics as a function of the pulling velocity v_0: stick-slip (relaxation) motion and damped harmonic motion. In Fig. 2(a) we see a typical example of the stick-slip motion described in the Introduction. When the slope of the signal is positive, the block is stuck. When the force on the spring reaches a critical force (the slip force), the block slides and then comes to rest again relative to the surface (the stick force). The "discontinuities" representing these slip events have, of course, a finite width (the slip duration). The damped harmonic limit is shown in Fig. 2(b). A discussion of these data will be presented in Sec. V D.

There are two methods of data analysis. The first is to simply take a power spectrum of the raw data. For the longest runs, we were able to measure frequencies down to 32 μHz. The second method is to sort the raw data for events only. This was done with the DSA by sampling the raw signal at 82 Hz and storing this sampled data on disk. Using this method, the maximum measurement time was ~ 2.5 h due to disk space limitations. These data were then run through an algorithm which searched them for potential events. To identify an event, the algorithm used the derivative of the curve as the triggering criterion. Since excess noise (e.g., at the line frequency)

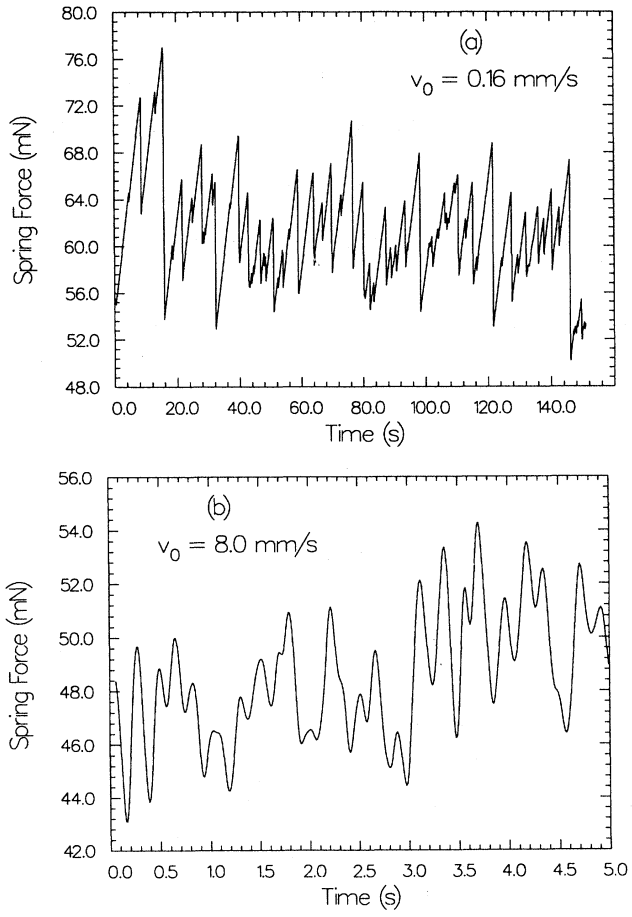

FIG. 2. The spring force as a function of time showing the two limiting cases for the dynamics. (a) Stick-slip (relaxation) motion; (b) damped harmonic motion (continuous sliding).

will also trigger the algorithm, a mean filter was applied and a second criterion was used to identify an event, namely the duration of the slip. Slips with durations less than or equal to three sample intervals (≈ 0.04 s) were rejected. This algorithm was applied to various data sets and checked by eye. No obvious events were missed and nothing that was indistinguishable from the noise was selected. When an event was located, the following four event parameters were recorded: the event time, the slip size, the slip force, and the slip duration. In the data sets that will be presented, all had more than 35 000 events, except those with $v_0 = 0.016$ mm/s which had ~ 6000 events.

To what extent are the data reproducible? Due to factors such as wear and oxidation, the raw signal will never be exactly reproducible in the sense that a run over the same surface segment will yield the same result. Nevertheless, averaged quantities, such as the distributions of the event parameters and the power spectra, were always found to be reproducible. This also implies that we are observing a stationary process at least on the time scales of the experiment. Eventually, of course, significant wear will occur which will alter the dynamics.

V. EXPERIMENTAL RESULTS

The system was studied primarily with three configurations:

(i) Small mass (28.5 g) and loose spring (22.4 N/m): $v_D = 350$ mm/s.

(ii) Small mass (28.5 g) and stiff spring (152 N/m): $v_D = 134$ mm/s.

(iii) Large mass (670 g) and stiff spring (152 N/m): $v_D = 651$ mm/s.

The meaning of v_D will be discussed in Sec. VI. Only the stick-slip (relaxation) regime will be examined in the following sections. An analysis of the damped harmonic (continuous sliding) regime will be deferred until Sec. V D. Unless indicated otherwise, the steel surface was used. Configuration (i) was also studied with the aluminum and brass surfaces.

A. Configuration (i)

We return once again to the data segment shown in Fig. 2(a) which was in fact taken with this configuration. The following qualitative features should now be noted. First, there is no apparent periodicity in the signal. This implies that the friction force might not obey a simple deterministic relation. This is supported by the fact that slip forces of approximately the same magnitude can be followed by considerably different slip sizes. Second, there are slip sizes covering the full dynamic range of our measuring apparatus. Finally, it appears that there is a build-up preceding a large slip, i.e., there are a number of small jumps just before a large one. We will now examine the distributions of some of the event parameters. All of the distributions that will be presented have been normalized.

1. Slip size distribution

This is the most obvious one to study given its possible connection to single fault slips in earthquakes (see Appendix). In our system, we can explicitly calculate the relationship between the energy E released (dissipated) in a slip and the slip size s. If the block is at rest (in the table's frame of reference) just before and just after an event, then the energy released is just the change in the potential energy of the spring:

$$E = \frac{k}{2}\left[(x_2 - \ell)^2 - (x_1 - \ell)^2\right], \tag{2}$$

where k is the spring constant, ℓ is the equilibrium length of the spring, and x_2 and x_1 are the positions of the block just before and just after an event, respectively. Since $s = x_2 - x_1$, we can rewrite Eq. (2) as

$$E = k\,s\,[x_2 - \ell - s/2]. \tag{3}$$

Thus, if $x_2 - \ell \gg s/2$ we find that $E \sim s$, as assumed for earthquakes. In our experiment, this condition only fails for the very largest (and rarest) slips.

The distributions for the slip size are shown in Fig. 3 for a wide range of pulling velocities. (The statistics are such that it is not necessary to show the cumulative distributions as is usually done.) It appears that they have an approximately exponential distribution with a characteristic size of ~ 0.1 mm which is independent of the pulling velocity v_0. For this configuration, we do not observe the scaling seen in earthquakes, model systems, or simulations.

It should be pointed out that the slip size can be defined either in the laboratory frame of reference or in the table's frame of reference. As $v_0 \to 0$, they become indistinguishable, but this is not true otherwise. However, the corrections for $v_0 \sim 0.3$ mm/s are typically $\lesssim 0.01$ mm and hence insignificant. The distributions shown in Fig. 3 are for the laboratory frame which is consistent with Eq. (2).

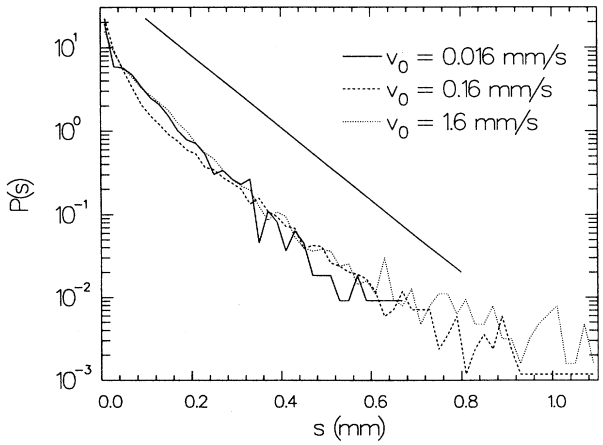

FIG. 3. Slip size distributions for configuration (i). The straight line above the data is a decaying exponential function with a decay length of 0.1 mm.

A Poisson process, i.e., where there is a uniform probability that the block will stick in an interval ds, will, of course, yield an exponential distribution. However, this cannot be the complete explanation for the data. This can most clearly be seen by looking at the return plot of the slip size *difference*, i.e., $s_{n+1} - s_n$ vs $s_n - s_{n-1}$. This is shown in Fig. 4. (One can also see correlations in the slip size return plot, i.e., s_{n+1} vs s_n, but it is not nearly as striking as Fig. 4.) The interpretation for this figure concerns the build-up discussed at the beginning of this section. Consider a sequence of three consecutive slips. Three small slips will result in the clustering of points near the origin. Two small slips followed by a large slip will result in the clustering of points on the positive y axis. A large slip followed by two small slips will result in the clustering on the negative x axis. A small slip followed by a large slip followed by a small slip results in the clustering on the line $y = -x$ in the fourth quadrant. If the slip sizes were indeed randomly distributed, i.e., uncorrelated with one another, they would produce a circularly symmetric distribution. Thus, although the distributions appear to be exponential, the underlying dynamics may not be Poissonian.

The slip size distributions for the aluminum and brass surfaces are qualitatively similar to the data taken on the steel surface, except that the characteristic length is larger. As examples, the distributions for $v_0 = 0.16$ mm/s are shown in Fig. 5.

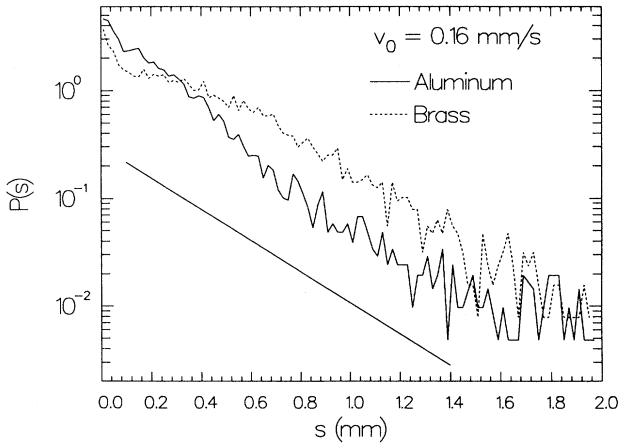

FIG. 5. Slip size distributions for aluminum and brass for configuration (i). The straight line below the data is a decaying exponential function with a decay length of 0.3 mm.

2. *Slip force distribution*

The slip force distributions are shown in Fig. 6. If we consider the local static friction to be a function of position, then the slip force is probing this function. For $v_0 \lesssim 0.4$ mm/s, the slip force (static friction) distribution is well parametrized by a three-parameter log-normal distribution:

$$P(f) = \frac{1}{\sqrt{2\pi}\sigma(f - f_c)} \times \exp\left[-\frac{[\ln(f - f_c) - \ln(f_0 - f_c)]^2}{2\sigma^2}\right], \quad (4)$$

where f_0 is the peak position, f_c is a lower threshold, and σ is a measure of the width of the distribution. The significance of f_c is that there exists a lower threshold for the static friction. It is not easy to explain the presence of a significant tail, let alone why the static friction in the experiment should follow such a distribution. Log-normal distributions can be a consequence of, for example, the law of proportionate effect, and one can easily make arguments in this vein. However, this is not very rewarding in terms of new insight.

As we increase v_0, the log-normal fit becomes worse. If we attribute the log-normal distribution to the static

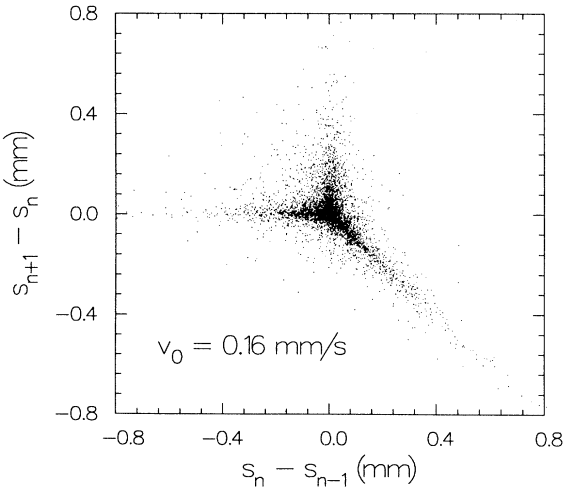

FIG. 4. Return plot of the slip size difference for configuration (i).

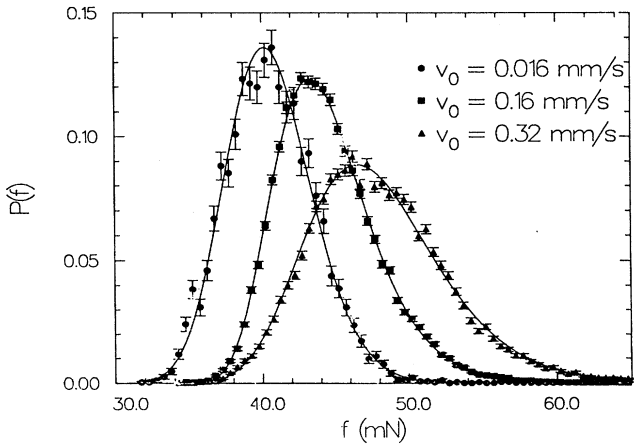

FIG. 6. The slip force distributions for configuration (i). The solid lines are fits to log-normal distributions (see text).

friction, then there is no reason why it should parametrize the slip force at faster velocities since there is no longer a simple correspondence between the slip force and the static friction.

We note that the static coefficient of friction, defined as the mean static friction (approximately the peak position) divided by the load, is ≈ 0.15 in agreement with previous results [3]. Also, the threshold f_c for the static friction decreases with decreasing velocity and is independent of the surface material. This indicates a two-parameter log-normal distribution for the static friction in the limit $v_0 \to 0$.

This brings us to the question of whether the slip force distribution, which is the measured static friction, can be interpreted more generally as the true distribution for the static friction. The question is relevant since we do see a velocity dependence in the log-normal distributions. The reason for this may be that the dynamics are deciding how we are probing the surface, e.g., there may be strong correlations between the slip force f and the stick force $f - ks$. The distribution of conditional probabilities $P(f - ks|f)$ seen in Fig. 7 indicates that the correlations are weak since the slip force does not determine the lowest value for the stick force. This does not, however, rule out an exclusion process. One interpretation is that due to the *average* velocity dependence of the dynamic friction, the slipping will cease at a higher spring force when the velocity of the table is higher. Hence the dynamics are not directly deciding how we are probing the surface, but are excluding a part of the true static friction distribution that can only be measured by placing the block at random positions and then pulling it.

The slip force distributions for aluminum and brass are also well parametrized by log-normal distributions. As examples, the distributions for $v_0 = 0.16$ mm/s are shown in Fig. 8.

3. *Waiting time distributions*

If the nth event begins at time t_n, then the waiting time is defined as $\Delta_n = t_{n+1} - t_n$. The waiting time distributions for two intermediate velocities are shown in Fig. 9. They are peaked and appear to have exponential tails whose slopes are clearly dependent on v_0, as expected. (A pure exponential is expected for a Poisson process, i.e., random events.) For the slowest velocity we see more complicated behavior, as shown in Fig. 10. For waiting times $\lesssim 2$ s, there is a possibly exponential decay before the peak. It would appear therefore that there may be different processes dominating on different time scales.

If we compute the average time τ between two events, $\tau = \frac{1}{N}\sum_{n=1}^{N-1}\Delta_n$, it depends on the pulling velocity v_0 as shown in Fig. 11. These data can be explained as follows. Clearly, the waiting time is a sum of the time spent sticking to the table surface plus the time spent sliding on it (the slip duration). If we then assume that both the average distance the spring stretches (or equivalently, the force in the spring increases) and the average time spent sliding are independent of v_0, then $\tau(v_0)$ can be written

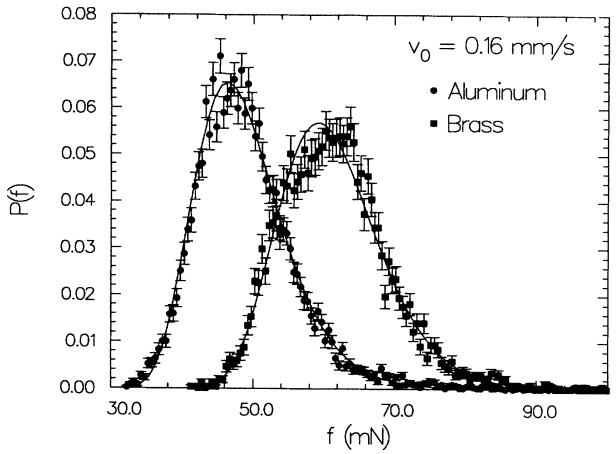

FIG. 8. Slip force distributions for aluminum and brass for configuration (i). The solid lines are fits to log-normal distributions.

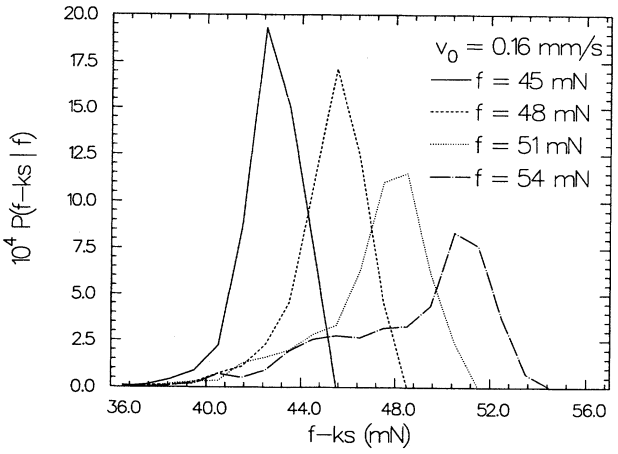

FIG. 7. Conditional probability $P(f - ks|f)$ for configuration (i).

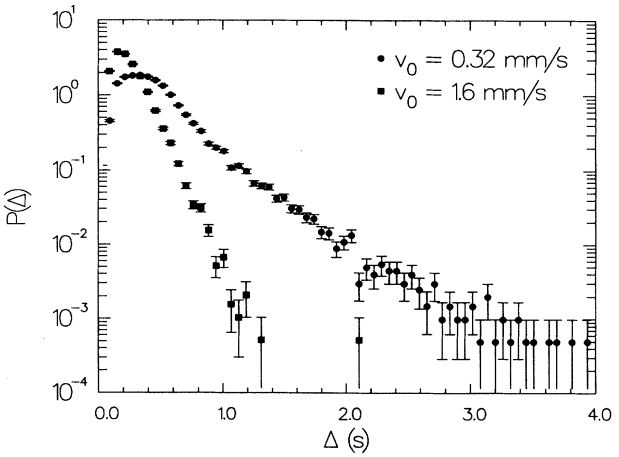

FIG. 9. Waiting time distributions for configuration (i).

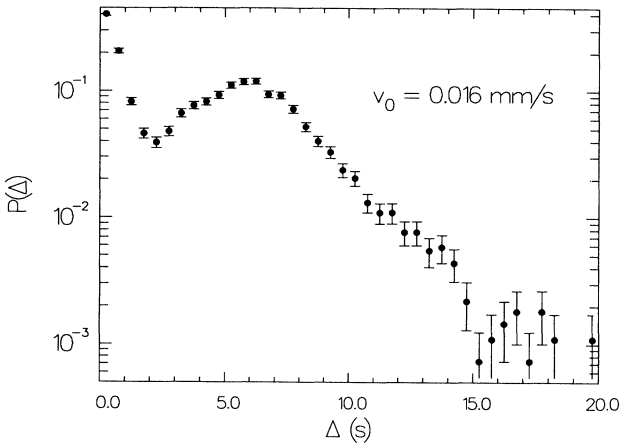

FIG. 10. Waiting time distribution for the slowest velocity for configuration (i).

as

$$\tau(v_0) = \frac{\delta}{v_0} + \tau_\infty, \tag{5}$$

where δ is the mean distance the spring stretches during sticking, and τ_∞ is the mean slip duration. Equation (5) also yields the correct asymptotic behavior. As $v_0 \to \infty, \tau \to \tau_\infty$ where τ_∞ is found experimentally to be within 5% of the undamped eigenperiod $2\pi\sqrt{m/k}$, and as $v_0 \to 0, \tau \to \infty$, as one would expect. This agrees with previous results showing that the frequency of the motion approaches that of the undamped eigenfrequency as the pulling velocity is increased [4].

4. *Power spectra*

Power spectra can be a useful although somewhat limited tool in analyzing dynamic phenomena. Specifically, it only measures two-point correlations and thus is not sensitive to higher-order correlations that are apparent, for example, in Fig. 4.

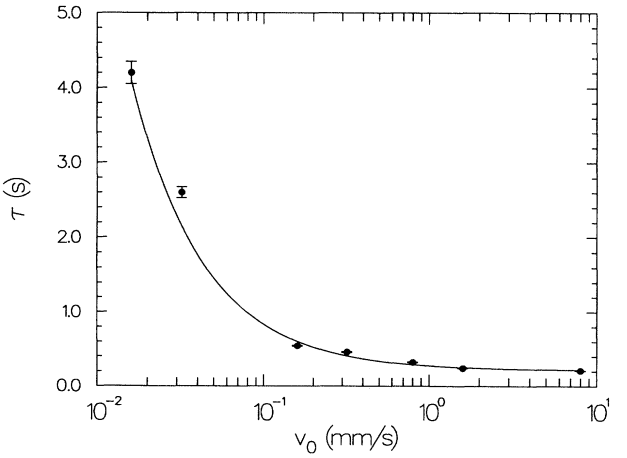

FIG. 11. The average waiting time $\tau(v_0)$ for configuration (i). The solid line is a fit to Eq. (5) giving $\delta = 0.06$ mm and $\tau_\infty = 0.21$ s.

The stick-slip motion typified in Fig. 2(a) can be represented by the following expression for the position of the block as a function of time in the laboratory frame of reference:

$$x(t) = x_0 + v_0 t - \sum_{n=1}^{N} s_n \theta(t - t_n) \ , \tag{6}$$

where a is a constant, N is the total number of events, s_n and t_n are the size and time of the nth event, respectively, and $\theta(t)$ is the step function. Thus we assume that the signal consists of a linear part interrupted by instantaneous events, which becomes a better approximation to the true signal as $v_0 \to 0$. (Of course, the slips are not instantaneous, but we will ignore this since it only results in some form-factor effects not relevant to the present analysis.) With periodic boundary conditions with period T, the Fourier transform of $x(t)$ is (ignoring the constant x_0)

$$\tilde{x}(\omega) = \frac{1}{i\omega}\left[v_0 T - \sum_{n=1}^{N} s_n + \sum_{n=1}^{N} s_n e^{i\omega t_n}\right]. \tag{7}$$

Now, the first two terms inside the brackets will tend to cancel, since this is precisely the condition for the dynamics to be stationary. Thus the power spectrum is just

$$S(\omega) \equiv |\tilde{x}(\omega)|^2 = \frac{1}{\omega^2}\left[\sum_{n=1}^{N} s_n^2 + \sum_{n \neq m}^{N} s_n s_m e^{i\omega(t_n - t_m)}\right], \tag{8}$$

where the first term inside the brackets represents the self-correlations. At high frequencies only the self-correlations will remain, yielding the expected $1/f^2$ behavior originating from the slip discontinuities. At sufficiently low frequencies, the terms inside the brackets will become constant, so again one should observe $1/f^2$ behavior. What will happen in between will be determined by the specific correlations between the s_n's and t_n's.

If the s_n's and Δ_n's are uncorrelated for different events and with each other, then it can be shown that the power spectrum becomes [26, 27]

$$S(\omega) \sim \frac{1}{\omega^2}\left[1 + 2\frac{\langle s\rangle^2}{\langle s^2\rangle}\mathrm{Re}\frac{\psi}{1-\psi}\right]$$
$$\psi = \int_0^\infty P(\Delta) e^{-i\omega\Delta} d\Delta \ , \tag{9}$$

where $\langle s\rangle^2$ and $\langle s^2\rangle$ are the first and second moments of the slip size distribution respectively, and $P(\Delta)$ is the waiting time distribution. In this case, we see that we only require the distributions for s and Δ in order to calculate the power spectrum.

The power spectra for steel, aluminum, and brass at two different velocities are shown in Figs. 12(a) and 12(b), respectively. Using a model function for the measured waiting time distributions shown in Figs. 9 and 10,

it is possible to find a numerical solution to Eq. (9), but it misses all the important features of the data. It does not reproduce either the position or the size of the shoulders in the data or, more importantly, the low-frequency behavior. [Other (deterministic) assumptions concerning the interdependence of s_n and Δ_n can be made [27], but it does not improve matters.] Instead we see nontrivial long-time correlations indicating that $S(f) \sim f^{-\alpha}$ with α between 1 and 1.3.

We note that $1/f^2$ behavior is still expected at some lower frequency. However, if we measure for too long, correlations from the finite size of the table result in a peak in the power spectrum corresponding to the period of rotation. This makes longer time measurements impossible. These correlations are shown in Fig. 13 for $v_0 = 8.0$ mm/s although it was observed at all velocities. The first and strongest peak is from the period at ≈ 125 s, and the higher frequency peaks are its harmonics. The shape and width of the peaks correspond to an exponential decay time for the autocorrelation function of ~ 80 s. There are clearly memory effects in the stick-slip process, indicating, for example, that the stick-slip characteristics are local properties of the surface.

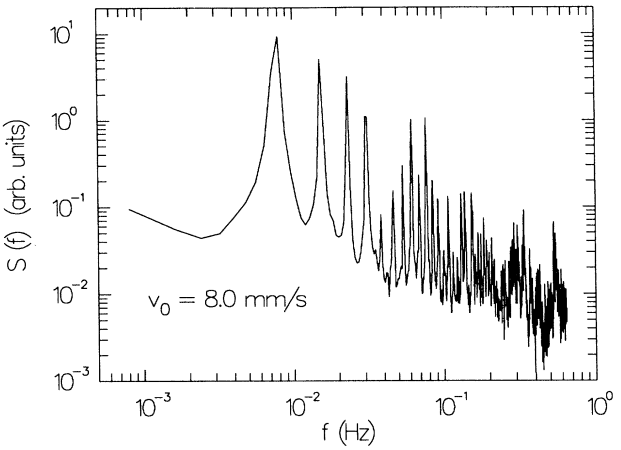

FIG. 13. Power spectrum for configuration (i) showing correlations corresponding to the period of rotation of the table.

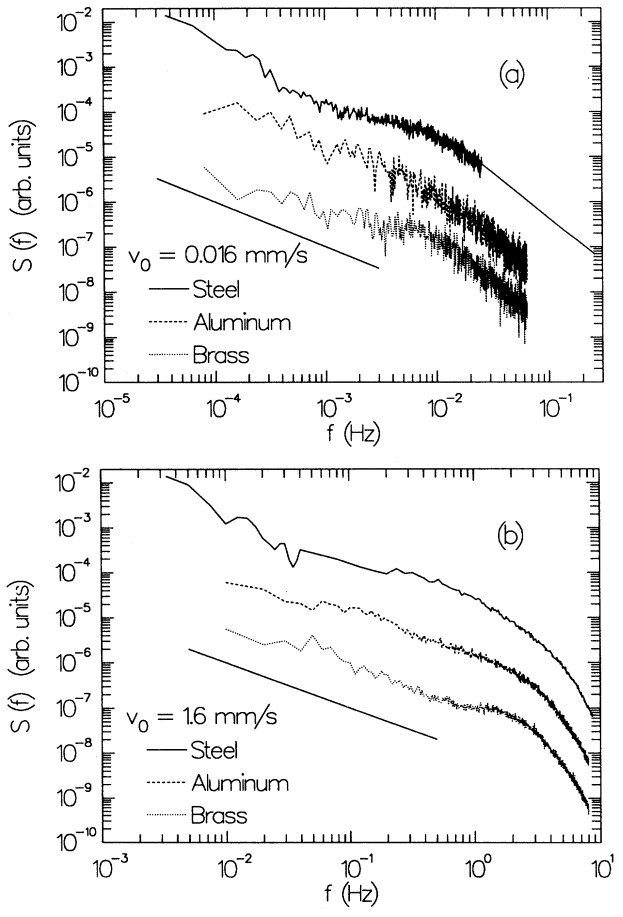

FIG. 12. Power spectra for steel, aluminum, and brass for configuration (i). (a) $v_0 = 0.016$ mm/s. The steel data is composed of two separate measurements, the high frequency part being heavily averaged. (b) $v_0 = 1.6$ mm/s. The straight lines below the data are a power law with an exponent of -1.

B. Configuration (ii)

When we used a stiffer spring with the same small mass, we found qualitatively different behavior. Figure 14 shows the slip size distribution for this configuration. It is no longer exponential and would appear to be better represented by a power-law distribution. For comparison, the slip size distributions for configuration (i) (see Fig. 3) are also included here. Unfortunately, it was not possible to examine this development further since the measureable range of motion of the block becomes increasingly restricted as the ratio of m/k is decreased.

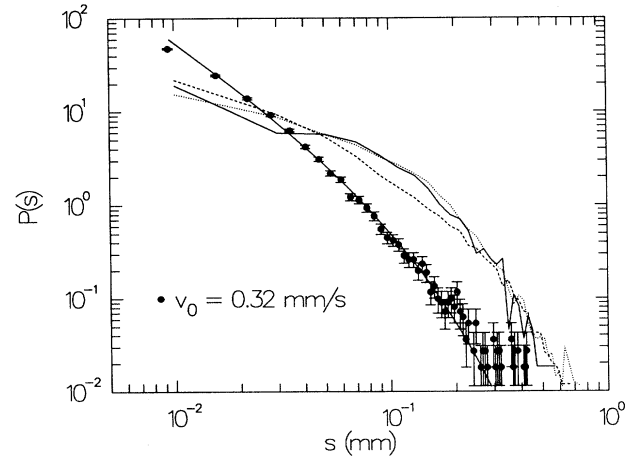

FIG. 14. Slip size distribution for configuration (ii). The solid line through the data is a fit to Eq. (10) (see text). The slip size distributions for configuration (i) (see Fig. 3) are also shown for comparison.

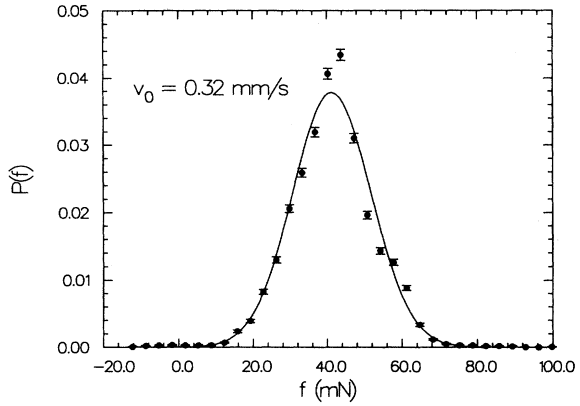

FIG. 15. Slip force distribution for configuration (ii). The solid line is a fit to a Gaussian distribution.

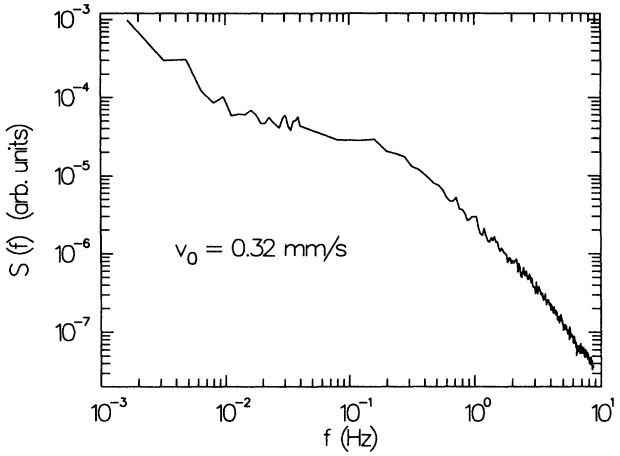

FIG. 17. Power spectrum for configuration (ii).

It will be observed that there is a small curvature in the data, indicating that a power-law distribution must be modified. One obvious choice is

$$P(s) \sim s^{-\beta} e^{-s/s_c}, \tag{10}$$

where s_c is a cutoff length. A fit to this function is shown in Fig. 14 and yields $\beta \simeq 1.6 \pm 0.3$ and $s_c \simeq 0.1 \pm 0.05$ mm. The corresponding exponent found in earthquakes (see Appendix) ranges from 1.6 to 2 for small and large earthquakes, respectively. What is the meaning of s_c? If it is a correlation length, then we should interpret configurations (i) and (ii) as, respectively, the "hydrodynamic" and "critical" regimes of the same fixed point.

The slip force distribution is shown in Fig. 15. The distribution would now appear to be symmetric, lacking the tails seen in Fig. 6 for configuration (i). In Fig. 16 we show the waiting time distribution. It still has a peak and an exponential tail as in configuration (i). The power spectrum is shown in Fig. 17. It is difficult to conclude anything about the low frequency behavior.

C. Configuration (iii)

From the discussion of contact area in Sec. II A, we expect more deterministic (and hence periodic) behavior as the block mass is increased. (The spring constant was also necessarily increased.) In Figs. 18–20, we show the distributions for the slip size, slip force, and waiting time, respectively. They all appear to be Gaussian and hence we conclude that the motion is quasiperiodic in agreement with previous results [4]. The power spectrum shown in Fig. 21 corroborates this conclusion. The peak at ~ 0.3 Hz corresponds to the mean waiting time seen in Fig. 20.

D. Langevin model for large v_0

We now recall the colliding asperity model for dynamic friction discussed in Sec. II B. As the block slides across the table, there will be many collisions between the as-

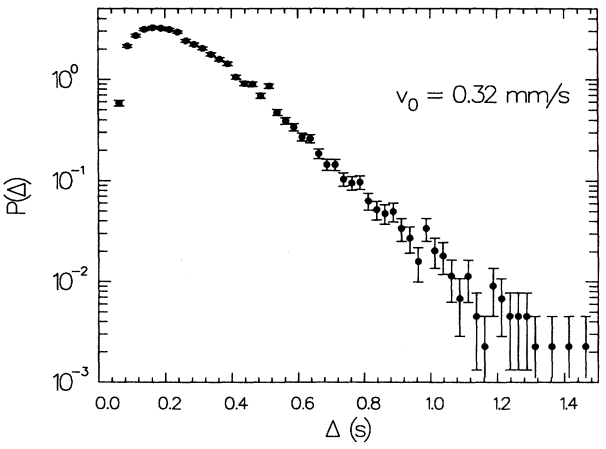

FIG. 16. Waiting time distribution for configuration (ii).

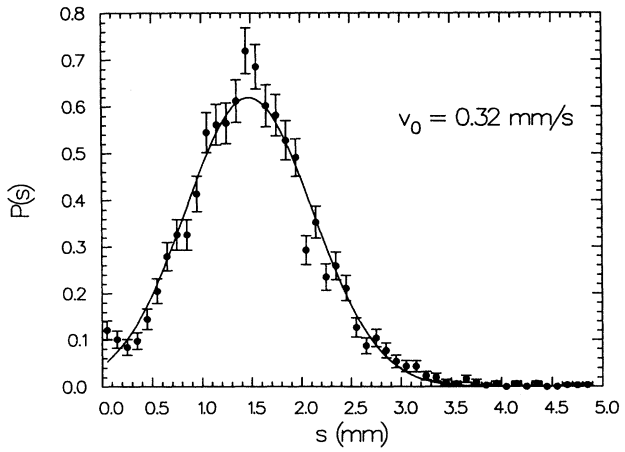

FIG. 18. Slip size distribution for configuration (iii). The solid line is a fit to a Gaussian distribution.

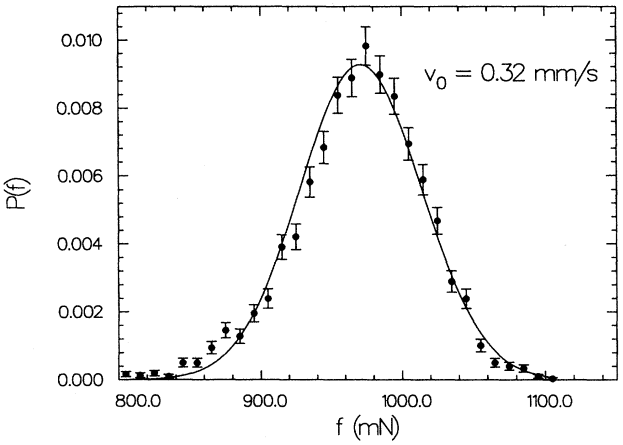

FIG. 19. Slip force distribution for configuration (iii). The solid line is a fit to a Gaussian distribution.

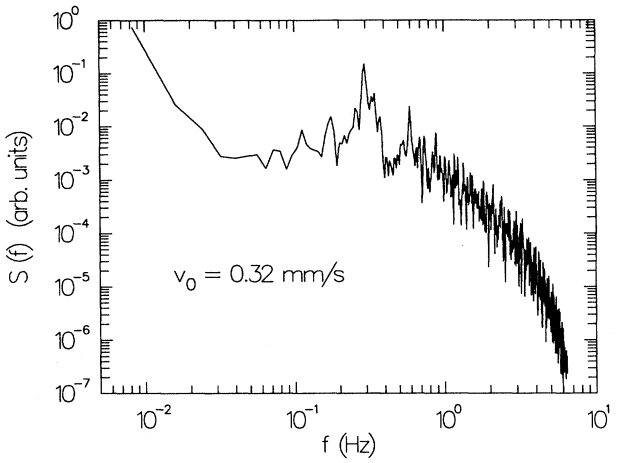

FIG. 21. Power spectrum for configuration (iii).

perities of the two surfaces. Since the asperities have a spacing $\gtrsim 5$ μm [23], the block will, on average, cover hundreds of asperities per second as it slides across the surface. This makes it reasonable to think of the motion of the block as generating noise. We therefore propose the following equation of motion for the position $x(t)$ of the block in the laboratory frame of reference:

$$\ddot{x} + \gamma(\dot{x} - v_0) + \omega_0^2 x = (\dot{x} - v_0)\eta(t), \tag{11}$$

where γ is a damping coefficient ($\gamma\dot{x}$ may be regarded as the linear term of an expansion), $\omega_0 = \sqrt{k/m}$ is the natural frequency, and $\eta(t)$ is a Gaussian noise term, i.e., $\langle\eta(t)\rangle = 0$ and $\langle\eta(t)\eta(t')\rangle = 2D\delta(t - t')$. The form of Eq. (11) is such that both the damping and the noise will vanish when the block is at rest relative to the table. Substituting $y = x - \gamma v_0/\omega_0^2$, we can rewrite Eq. (11) as

$$\ddot{y} + [\gamma - \eta(t)]\dot{y} + \omega_0^2 y = -v_0\eta(t). \tag{12}$$

We believe that the noise term modifying the damping will have no effect except at short times. (This appears to be confirmed by simulations.) Thus, Eq. (12) will simply behave as a Langevin equation for a noise-driven damped harmonic oscillator. The power spectrum is then just [28]

$$S(\omega) = \frac{4D}{|-\omega^2 + i\gamma\omega + \omega_0^2|^2}. \tag{13}$$

Figure 22 shows the power spectrum for configuration (i) with $v_0 = 8.0$ mm/s. There appears to be a $1/f^2$ background. This is most likely an artifact of making a finite time measurement which can create the illusion of a slow constant drift in the signal. That is, if $x(t) \to x(t) + ct$ then $\tilde{x}(\omega) \to \tilde{x}(\omega) + c/i\omega$ (for periodic boundary conditions) resulting in the addition of a $1/\omega^2$ term to Eq. (13). In Fig. 22 is also shown a fit to the data of Eq. (13) with this correction term added and with ω_0 fixed to its measured value.

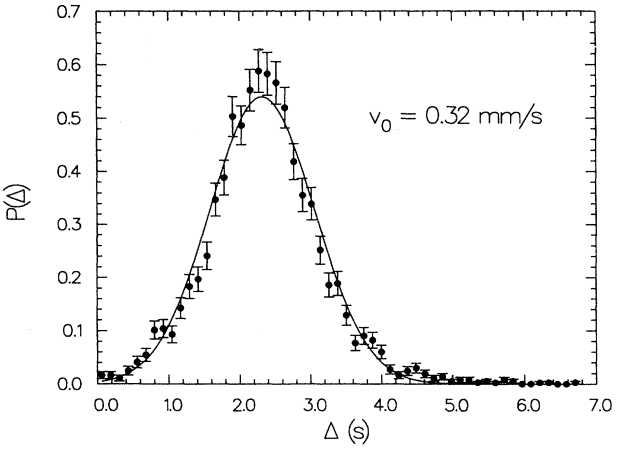

FIG. 20. Waiting time distribution for configuration (iii). The solid line is a fit to a Gaussian distribution.

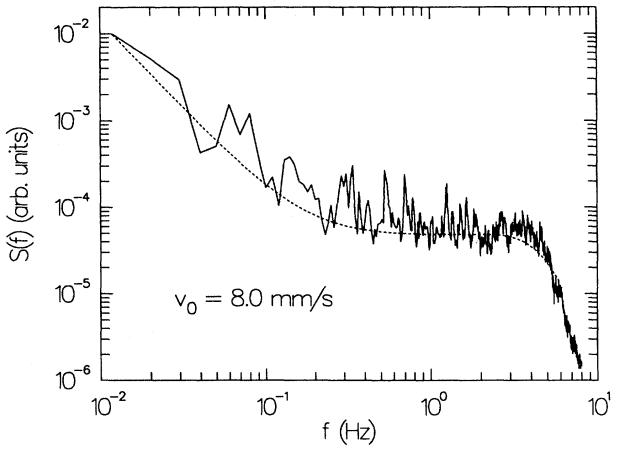

FIG. 22. Power spectrum for continuous sliding for configuration (i). The dashed line is a fit to Eq. (13) corrected for a linear drift (see text).

VI. DISCUSSION

Following Vasconcelos *et al.* [14], we will assume that the dynamics is determined by the various scale velocities found in the problem. In our case, there are two. First, there is the pulling velocity v_0. Dimensionally, we can form a second velocity from the available parameters, which is $v_D = g\sqrt{m/k}$. The physical meaning of v_D is that it is proportional to the maximum velocity that can be attained by the block when it slips. If we consider the motion of the block when it is sliding to be that of an undamped harmonic oscillator, then its position as a function of time is $x(t) = x_0 \cos\omega_0 t$ where x_0 is the initial position of the block, and of course $\omega_0 = \sqrt{k/m}$. Its velocity is therefore $\dot{x}(t) = -x_0\omega_0 \sin\omega_0 t$. The initial position x_0 is just the displacement of the spring when the block slips, which is just the slip force divided by the spring constant, i.e., $x_0 = f/k$. The slip force is given by $f = \mu_s mg$ where μ_s is the static coefficient of friction the instant before a slip begins. Thus, the maximum velocity of the block is $x_0\omega_0 = \mu_s g\sqrt{m/k}$.

We would now like to consider our system in the context of a dynamic phase diagram, with the pulling velocity v_0 and the dynamic velocity v_D as the phase parameters. The phase diagram might then look schematically like Fig. 23. Clearly, for sufficiently large v_0, the block is continuously sliding over the surface. One might suppose that as v_D is increased, this will only happen for larger and larger values of v_0. As $v_0 \to 0$, we see only stick-slip (relaxation) motion. For large values of v_D [configuration (iii); see Sec. V], we observe nearly periodic motion. As v_D is decreased [configuration (i)], the motion becomes aperiodic and has approximately an exponential slip size distribution. As v_D is decreased further [configuration (ii)], the slip size distribution becomes distinctly nonexponential and possibly power-law, indicating a crossover from a "hydrodynamic" to a "critical" regime. The nature of the boundaries is not known, although they are certainly not sharp. For example, we know there is a region between continuous sliding and stick-slip motion which is a mixture of the two. In this case, one might regard the fraction of time spent sticking as an order parameter [14].

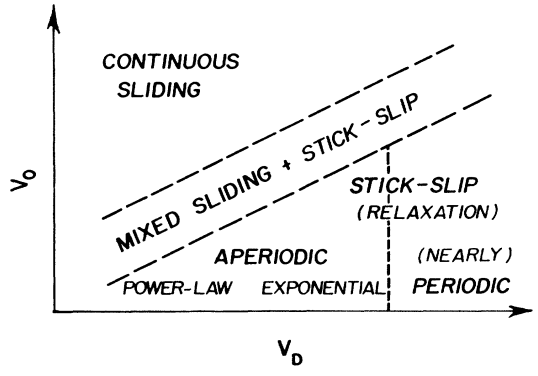

FIG. 23. A schematic of the dynamic phase diagram for the spring-block system (see text).

The physical consequences of changing v_D can be speculated upon as follows. If we regard the block as a point object moving in a potential well due to the interactions of the asperities, then for sufficiently large v_D, the block will always have sufficient energy to clear every energy barrier, since the asperities obviously have a maximum size. In this case, the dissipation mechanism is independent of the asperity size distribution, i.e., only average values are important, resulting in a more or less deterministic friction force and hence (nearly) periodic motion of the block. As v_D is decreased, the block will interact with the larger asperities, resulting in stochastic behavior reflecting their distribution. As v_D is decreased yet further, the block interacts with even the smallest asperities from which we must conclude from the data that they have a different distribution than the large asperities.

The one-dimensional model of Jensen *et al.* [29], where a chain of particles interconnected by springs moves in a random potential, yields some results similar to ours. However, it is not straightforward to map our experiment onto this model. They find a power spectrum qualitatively similar to those in Fig. 12 and an asymmetric slip force distribution as we do. However, their slip size distribution appears to be power-law and not exponential. It may be that their system will display exponential slip size distributions in some other region of their parameter space.

The onset of a slip might be considered in the context of the so-called fiber-bundle model of which there are two versions. The first is "democratic," where after the breaking of one fiber the force is redistributed equally among the remaining fibers. It can be shown [30] that this version obeys a central limit theorem yielding a Gaussian distribution of the breaking force for the entire bundle. The other version is "hierarchical," where the weakest fiber breaks first, the second weakest next, and so forth. Hence, the force for which the bundle breaks is given by the strongest fiber. For a rather general class of distribution of fiber strengths, this will yield an extreme value distribution for the breaking force of the entire bundle. Thus, neither version reproduces the log-normal distributions found in our experiment.

ACKNOWLEDGMENTS

The authors would like to thank C. Bech, H. Flyvbjerg, G. Grinstein, T. Guhr, C. Jayaprakash, S. Nagel, T. Schreiber, and S. Solla for many illuminating discussions. They are particularly grateful to J. Jacobsen for providing them with the steel bearing, and for educational conversations concerning friction. We especially thank H.J. Jensen for providing us with details of his work. P.D. would like to thank the SARC Fond, Ib Henriksens Fond, Statens Naturvidenskabelige Forskningsred (Danish Science Foundation), Novos Fond, the Leon Rosenfeld Fond, and the Niels Bohr Institute for support. A.J. thanks Novos Fond for support and the Niels Bohr Institute for hospitality. H.H.R. thanks the CROUS/DRED under the French government and the Danish Natural Science Research Council for financial support.

APPENDIX: EARTHQUAKES

A great deal has been written about earthquakes [31]. For reference, we briefly review some of the pertinent concepts. The seismic moment is often defined as $M = \mu s A$ where μ is an elastic shear modulus, s is the size of a fault slip, and A is the area of the fault. The seismic energy E is proportional to the seismic moment. The Gutenberg-Richter law states that the cumulative number of earthquakes N_c greater than a magnitude m is given by $\log N_c = a - bm$ where a and b are empirical constants [32]. The magnitude and seismic moment are in turn related by $m = \frac{1}{c} \log M - d$, where c and d are again empirical constants. Thus, the number density n of earthquakes of energy E or event size s scales as

$$n \sim E^{-B-1} \sim s^{-B-1} ,$$

where $B = b/c$. There is some consensus that $B \sim 0.6$ for small earthquakes, while $B \sim 1$ for large earthquakes.

[1] F.P. Bowden and L. Leben, Proc. R. Soc. London Ser. A **169**, 371 (1939).

[2] F.P. Bowden and D. Tabor, *The Friction and Lubrication of Solids* (Clarendon Press, Oxford, 1950), Part 1 and (1964), Part 2.

[3] I.V. Kragelskii, *Friction and Wear* (Butterworth, Washington, DC, 1965).

[4] J.A.C. Martin and J.T. Oden, Comp. Meth. Appl. Mech. Eng. **52**, 527 (1985); J.A.C. Martin, J.T. Oden, and F.M.F Simões, Int. J. Eng. Sci. **28**, 29 (1990).

[5] E. Rabinowicz, *Friction and Wear of Materials* (Wiley, New York, 1965).

[6] I. Andersson, Ph.D. thesis, University of Chalmers, Sweden (1980).

[7] W.F. Brace and J.D. Byrlee, Science **153**, 990 (1966).

[8] R. Burridge and L. Knopoff, Bull. Seis. Soc. Am. **57**, 341 (1967).

[9] J.M. Carlson and J.S. Langer, Phys. Rev. Lett. **62**, 2632 (1989); Phys. Rev. A **40**, 6470 (1989).

[10] J. Huang and D.L. Turcotte, Nature **348**, 234 (1990).

[11] Z. Olami, H.J.S. Feder, and K. Christensen, Phys. Rev. Lett. **68**, 1244 (1992).

[12] K. Christensen and Z. Olami, J. Geophys. Res. **97**, 8729 (1992).

[13] A. Crisanti, M.H. Jensen, A. Vulpiani, and G. Paladin, Phys. Rev. A **46**, R7363 (1992).

[14] G.L. Vasconcelos, M. de Sousa Vieira, and S.R. Nagel, Physica A **191**, 69 (1993). See also, M. de Sousa Vieira, G.L. Vasconcelos, and S.R. Nagel, Phys. Rev. E **47**, R2221 (1993).

[15] A. Johansen, Cand. scient. thesis, University of Copenhagen (1993).

[16] B.F. Feeny and F.C. Moon, Phys. Lett. A **141**, 397 (1989).

[17] P. Bak, C. Tang, and K. Wiesenfeld, Phys. Rev. Lett. **59**, 381 (1987); Phys. Rev. A **38**, 364 (1988).

[18] C. Tang and P. Bak, Phys. Rev. Lett. **60**, 2347 (1988).

[19] A. Sornette and D. Sornette, Europhys. Lett. **9**, 197 (1989).

[20] P. Bak and C. Tang, J. Geophys. Res. **94**, 15 635 (1989).

[21] H.J.S. Feder and J. Feder, Phys. Rev. Lett. **66**, 2669 (1991); **67**, 283 (1991).

[22] See, for example, F.P. Bowden and D. Tabor, Brit. J. Appl. Phys. **17**, 1521 (1966).

[23] J.F. Archard, Wear **113**, 3 (1986).

[24] A.L Ruina, J. Geophys. Res. **88**, 10 359 (1983).

[25] J. Lomnitz-Adler, J. Geophys. Res. **96**, 6121 (1991).

[26] P. Mazzetti, Nuovo Cimento **31**, 88 (1964).

[27] C. Heiden, Phys. Rev. **188**, 319 (1969).

[28] M.C. Wang and G.E. Uhlenbeck, Rev. Mod. Phys. **17**, 323 (1945).

[29] H.J. Jensen, Y. Brechet, and B. Doucot, J. Phys. I (France) **3**, 611 (1993).

[30] D. Sornette, J. Phys. A **22**, L243 (1989).

[31] For a recent review, see the contributions by P. Bak, C.H. Scholz, and D. Sornette, in *Spontaneous Formation of Space-Time Structures and Criticality*, Vol. 349 of *NATO Advanced Study Institute, Series C*, edited by T. Riste and D. Sherrington (Kluwer Academic, Dordrecht, 1991).

[32] B. Gutenberg and C.F. Richter, Ann. Geofis. **9**, 1 (1956).